行政院國家科學委員會補助專題研究計畫 □ 成 果 報 告
■期中進度報告

奈米世代 MOSFET 關鍵製程技術之研發(2/3)

計畫類別：■ 個別型計畫　□ 整合型計畫
計畫編號：NSC 92－2215－E－009－025
執行期間：92 年 08 月 01 日至 93 年 07 月 31 日

計畫主持人：羅正忠
共同主持人：葉清發
計畫參與人員： 陳永裕、陳添富、蕭智文、王碩晟。

成果報告類型(依經費核定清單規定繳交)：■精簡報告　□完整報告

本成果報告包括以下應繳交之附件：
□赴國外出差或研習心得報告一份
□赴大陸地區出差或研習心得報告一份
□出席國際學術會議心得報告及發表之論文各一份
□國際合作研究計畫國外研究報告書一份

處理方式：除產學合作研究計畫、提升產業技術及人才培育研究計畫、列管計畫及下列情形者外，得立即公開查詢
□涉及專利或其他智慧財產權，□一年□二年後可公開查詢

執行單位: 交通大學電子工程研究所

中　華　民　國　93　年　07　月　13　日

中文摘要

近年來，以氧化鋁為主的高介電材料已經逐漸取代傳統的閘極二氧化矽層，原因在於氧化鋁跟複晶矽閘極的相容性很高，且熱穩定性及微縮能力也很傑出。在計畫的第二年，我們研究以氧化鋁作為電晶體的閘極絕緣層，並使用快速熱退火技術來改善薄膜的電性與降低熱預算。此外，在進行後續熱處理的過程當中，矽跟高介電材料之間很容易成長出原生氧化層，因而大幅提高介電層的等效氧化層厚度，為了解決這個問題，我們也嘗試在沈積氧化鋁之前，先將矽基板表面以 800 度 1 小時的氨氣處理來抑制原生氧化層的成長。

在氧氣環境下的快速熱退火處理能夠有效地降低閘極漏電流，也會促進介面氧化層的成長，相對地，氮氣熱退火處理能夠填補氧化鋁薄膜內的斷鍵，並小幅降低表面粗糙度，此外，氨氣表面處理可以有效提高高介電氧化鋁薄膜的可靠度，藉著等效能障高度的提升，閘極漏電流也可以明顯地降低。

此外，我們接續第一年的成果，針對無塵室內來自空氣濾網當中的硼污染進行研究，目前使用的高效率空氣濾網多由玻璃纖維所製造，當它們在長時間使用下遭遇到氫氟酸的侵蝕時，就會放出硼離子，進而造成奈米元件的特性漂移。利用長時間之 HF 蒸氣的加速實驗和晶圓暴露實驗，輔以 TDS-APIMS 和 SIMS 量測，即可觀察到包括各種有機分子團和硼離子在 HF 蒸氣下的增加情況，又使用 PTFE 材質的空氣濾網則能夠有效地防止硼污染。

Abstract

Recently, MOSFETs with high-k gate dielectrics have been studied intensively and Al_2O_3 is a promising candidate because of its compatibility with the poly-Si gate process and relatively superior scalability. In the second year of this proposal, we utilized rapid thermal annealing technique to improve the quality of high-k film and reduce the thermal budget. Besides, a native oxide layer would easily formed at Si/Al_2O_3 interface during RTA process, resulting in significant increase of effective oxide thickness (EOT) and therefore we applied a NH_3 treatment at 800 degree C for 1 hr prior to Al_2O_3 deposition to suppress the growth of native oxide layer.

From the experimental data, it is obviously that O_2 penetration would induce the increase of the interfacial layer during RTA process. However, for samples with RTA in a N_2 ambient, the void-defect of sputtered Al_2O_3 film would be eliminated and the surface roughness after annealing also reduced. The dielectric reliability was enhanced with NH_3 pre-treatment. The conduction mechanism in Al_2O_3 thin film is dominated by Schottky conduction which occurred in the insulators with fewer defects and a more perfect metal-insulator interface. Samples after NH_3 treatment have higher barrier high to reduce the gate leakage current.

Besides, following the results of this proposal in the 1st year, we investigated the possible boron contamination from various HEPA and ULPA filters. Most commercial ULPA filters are made of glass-fiber, which may corrode in an acid vapor environment and release boron ions, resulting in the electrical property shifts of nano-devices. Through long term acceleration experiments and wafer exposure experiments in an bench with HF vapor, the increase of organic molecular and boron ions due to filter corrosion can be observed. The usage of PTFE ULPA filter can effectively prevent the boron contamination.

I. Introduction

Recently, MOSFETs with high-k gate dielectrics have been studied intensively and Al_2O_3 is a promising candidate because of its compatibility with the poly-silicon gate process and relatively superior scalability. As the dielectric constant of Al_2O_3 is higher than SiO_2, it will provide a significant increase in capacitance without scaling down the oxide thickness. Rapid thermal Annealing (RTA) is a short time processing technique that can contribute to reduce the thermal budget, low levels of surface roughness, and improve film qualities. Generally, there are many methods to passivate the Si surface such as surface nitridation, nitrogen-contained ambient annealing, or nitride deposition as the bottom layer. Nitridation of the Si surface using NH_3 treatment before the deposition of high-k materials has been shown to be effective in achieving the low EOT and preventing the boron penetration. However, this technique results in higher interface charges, which leads to higher hysteresis and reduced channel mobility. In this report, we studied the effect of suppressing interfacial layer growth by NH_3 surface treatments. The NH_3 treatment would nitridize the Si surface to form a silicon nitride layer. Silicon nitride is a superior barrier for H_2O and oxygen, and it can suppress oxygen to diffuse into Si substrate.

The cleanness of a clean room environment must be tightly controlled to achieve high-yield and high-performance ULSI manufacturing. Recently developed filters, such as HEPA and ULPA filters, effectively eliminate traditional contamination. However, the controllability of airborne molecular contamination (AMC) using present cleanroom technologies has not yet been validated because AMC is a kind of atomic or molecular level gas-phase contamination like organic and inorganic ones. In the near future, especially in the nanodevice era, contamination by organic compounds, inorganic ions and trace doping impurities in air in a cleanroom may dominate the characteristics, reliability, and even yield of devices. Acid vapor generated from the cleaning process is another important issue. Most commercial ULPA filters are made of glass-fiber, which may corroded in an acid vapor environment. Contaminants in a ULPA filter corroded by acid vapor will be released into the cleanroom air and adsorbed onto the surface of wafers, degrading the manufactured devices. Technologies for eliminating AMC from the manufacturing environment must be developed to solve these problems completely. Therefore, the development of a new filter material, which has minimal AMC and is resistant to acid vapor corrosion, is important to the fabrication of high-performance devices.

II. Experiments

(A) Al_2O_3 Gate Dielectrics Using Rapid Thermal Annealing Technology

The 6-inch P-type Si (100) wafers are cleaned by the RCA cleaning process. The high-k material Al_2O_3 was then deposited by reactive sputtering in Ar/O ambient. After Al_2O_3 deposition, a high temperature post deposition annealing is performed at 750℃, 850℃ and 950℃ respectively for 30 sec by RTA Rapid Thermal Annealing (RTA). In our experiment, the gate electrode formations were used the Physical Vapor Deposition (PVD) systems. We deposit the TiN film (2000Å) as the top gate electrode and the thermal evaporation system to deposit the Al film(5000Å) as the backside contact. The cross-sectional view and total experimental procedures of the structure were shown in Fig. 1. At last the Capacitance-Voltage (C-V) and Current-Voltage (I-V) characteristics were measured by HP-4284 and HP-4156C systems. The capacitance equivalent thickness (CET) was extracted from C-V curve.

(B) Al_2O_3 Gate Dielectrics using NH_3 Surface Nitridation Technology

First, the 6-inch P-type Si(100) wafers were cleaned with standard RCA clean. The samples were divided into two groups. One was without any surface treatment before Al_2O_3 deposition, and the other was with a NH_3 surface treatment before Al_2O_3 deposition. The NH_3-treatment is performed in high temperature furnace, 800℃ for 1 hour. After NH_3-treatment, a SiN_X layer(~10 Å) was deposited. Al_2O_3 dielectric was then deposited various thickness (30Å, 40Å, and 50Å) by reactive sputtering in the Ar/O (ratio = 24/1) ambient. After Al_2O_3 deposition, a high temperature post deposition annealing was performed at 900℃ in the O_2 or N_2 ambient. Finally, the gate electrode formation was performed by the Physical Vapor Deposition (PVD) systems. We deposited the TiN film (2000Å) as the top gate electrode and the thermal evaporation system to deposit the Al film (5000Å) as the backside contact. The cross-sectional view and total process flow were shown in Fig. 10. The Capacitance-Voltage (C-V) and Current-Voltage (I-V) characteristics were measured by HP-4284 and HP-4156C systems, respectively. The capacitance equivalent thickness (CET) was extracted from C-V curve. In order to study the conduction mechanism in the Al_2O_3 film, the current-voltage characteristics with various temperature were measured at room temperature (RT), 50℃, 75℃, 100℃, and 125℃, respectively.

(C) Evaluation of AMC through Air Sampling

A specially controlled and fabricated clean bench (CB) was set up in a clean room of class 10k. Figure 19(a) schematically depicts the CB. Clean room air, from the air inlet of the CB, was initially filtered through a filter module that included inorganic and organic ion chemical filters, before flowing through the main filter, which was designed to be changeable. Two main filters were used, the NEUROFINE PTFE filter (PTFE) and the glass-fiber ULPA filter (GF). The air flow rate and turnover rate inside the CB were set to 0.4 m/s and 5 %, respectively. The exposure experiments were conducted in a 1ppm HF vapor environment.

Figure 19(b) presents the air sampling tools, Impinger and TENAX, which were equipped with a flow meter and a pump. The flow rate and sampling time of Impinger were 2 L/min and 24-72 hrs while those of TENAX were 100 mL/min and 5 hrs. Impingers collected mainly both metals and boron elements. These were analyzed using an inductively coupled plasma mass spectrometer (ICP-MS). Organic substances were collected by a TENAX (a kind of absorbent) tube, and quantitatively analyzed by gas chromatograph mass spectrometer (GC-MS). The air in the CR was also analyzed for comparison. Table 2 summarizes the air sampling experimental conditions.

(D) Evaluation of AMC through Wafer Sampling

The AMC absorbed on the surfaces of actual 6” P-type (100) Si wafers was analyzed for each filter module. After standard RCA cleaning, wafers were divided into two parts, and exposed to the air in the CR and the CB for 24-72 hrs. The metal contaminants on these wafer surfaces were analyzed using total reflection X-ray fluorescence (TRXRF), while the organic contaminants were analyzed by thermal desorption system–atmospheric pressure ionized mass spectrum (TDS-APIMS). For comparison, the contamination of a wafer not exposed to any environment was evaluated as a control. Table 3 is the summary of wafer sampling experimental conditions.

III. Results and Discussion

(A) Al_2O_3 Gate Dielectrics Using Rapid Thermal Annealing Technology

After the Al_2O_3 deposition, the following processes may go through many high temperature treatments during the VLSI fabrication. Such high-temperature treatments are likely to change the morphology and properties of thin films. Fig. 2 and Fig. 3 shows the high frequency (100kHz) capacitance-voltage (C-V), and Fig. 4 shows the CET of Al_2O_3 samples (without surface treatment) after various post deposition annealing (PDA) temperature at 750℃, 850℃, 950℃ in the O_2 or N_2 ambient. The capacitance of Al_2O_3 samples annealing in an O_2 ambient decreases with the increasing annealing temperature. Therefore, the CET increases after annealing in an O_2 ambient. This is because an O_2 penetration will induce the increasing of the interfacial layer at Al_2O_3/Si-substrate and higher annealing temperature increasing will speed up interface layer growth rate. On the contrary, the capacitance of Al_2O_3 samples annealing in a N_2 ambient is increasing when annealing temperature increases. Therefore, the CET decreases after annealing in a N_2 ambient. The void-defects generated after the sputtered Al_2O_3 formation and it could be densified followed a RTA process in a N_2 ambient. The current density (J) in the J-E curve was defined by J = I / A, where A is the area of capacitor. The CET determined by the C-V measurement.

Fig. 5 shows the J-E characteristics of Al_2O_3 film with RTA process in an O_2 ambient. It shows that the thicker Al_2O_3 film will resist large leakage current, and the lower leakage current was observed. However, the thicker dielectric thickness will reduce capacitance and the driving current. Fig. 6 shows the J-V characteristics of the fabricated Al_2O_3 film with RTA in a N_2 ambient. The capacitor can have a lower leakage current with thinner CET. This is due to RTA process in a N_2 ambient can improve Al_2O_3 film by eliminating void-defect. Fig. 7 shows J versus PDA temperature in the O_2 and N_2 ambient. Obviously, higher PDA temperature can reduce leakage for both annealing ambient. Consequentially, the sputtered Al_2O_3 film can be improved after a N_2 RTA process. If the leakage current density in the oxide (J_{ox}) is kept constant during the stress test (implying that the applied current is held constant), the stress time to breakdown becomes the variable. The length of stress time t_{BD} elapsed until dielectric breakdown occurred. The time-to-breakdown behavior of a group of oxide samples under such test conditions is referred to as time-dependent dielectric breakdown (TDDB). The Weibull plot of charge to breakdown for Al_2O_3 samples with various PDA temperature in an O_2 ambient is shown in Fig. 8. Obviously, distribution of the samples with thinner CET is better than others. However, the level of the charge to breakdown is lower than we expect. Fig. 9 shows the Weibull plot of charge to breakdown for Al_2O_3 samples with various PDA temperature in a N_2 ambient. For various PDA temperatures, their distribution and charge to breakdown are almost the same and they are not dependent on Al_2O_3 thickness. This means that the interfacial layer determines the breakdown of the whole stack.

(B) Al_2O_3 Gate Dielectrics Using NH_3 Surface Nitridation Technology

Figure 11 shows the comparisons of the C-V curves of the samples with and without surface treatment after PDA 900℃ in an O_2 ambient. It is clear that samples with a NH_3 treatment had higher capacitance at strong accumulation than samples without a NH_3 treatment. The CET of Al_2O_3 film is effectively reduced after NH_3 nitridation since NH_3 surface can suppress the growth

of interfacial layer. In Fig. 11, we can also found the C-V curves shift negatively after NH_3 nitridation can be observed due to the nitridation-induced fixed positive charges. Since positive fixed charges in conventional NH_3 nitridation film is due to N–H bonds at the interface. Fig. 12 shows the comparisons of the C-V curves of the samples with or without surface treatment after PDA 900℃ in a N_2 ambient. We still can find that the CET of Al_2O_3 film is effectively reduced after NH3 treatment. However, the amount of the C-V curves shift negatively after NH3 nitridation is decreasing. The reason is due to that PDA in a N_2 ambient will enhance the magnitude of fixed charge in Al_2O_3 film Fig. 13 shows the variation of deposited thickness (measured by ellipsometer) versus CET after PDA 900℃ in an O_2 ambient. The NH3 treatment can effectively reduce the CET despite the initial oxide thickness, which shows the excellent CET scalability of this nitridation process. Because the presence of Si_3N_4 layer can effectively suppress the diffusion of oxygen species into the high-k/Si substrate interface. Without surface nitridation, Al and O atoms are easier to react with Si and are likely to form additional silicon dioxide and/or aluminum silicate layer with relatively lower k value. Fig. 14 shows the variation of Al_2O_3 thickness versus capacitance equivalent thickness (CET) after PDA 900℃ in a N_2 ambient. We can see almost the same result in an O_2 ambient as in a N_2 ambient, except in a N_2 ambient with higher k value. Figure 15 (a) and (b) show the relationship of gate leakage current versus gate bias after PDA 900℃ in the O_2 and N_2 ambient, respectively. The NH_3 –treatment samples show lower leakage current even with thinner CET. It is postulated that the NH_3-treatment can improve the quality of interface between high-k and silicon substrate and effectively reduce the leakage current. Fig. 16 shows the curve of Current density versus CET curves at Vg = -1V with NH_3 treatment and without NH_3 treatment. It is clear that NH_3 treatment can effectively reduce leakage current. Fig. 17(a) and (b) show the Weibull plots of the charge to breakdown (Q_{BD}) of Al_2O_3 samples with nearly the same CET after PDA 900℃ in theO_2 and N_2 ambient, respectively. The samples with NH_3 treatment shows more charge to breakdown (Q_{BD}). Thus, we suspect that surface nitridation may effectively reduce the concentration of oxygen vacancies during PDA due to its capability to suppress oxygen diffusion. On the other hand, the stronger Si-N bonds bring a stronger interface layer. When part of voltage drop across the Si_3N_4 interfacial layer in samples, the voltage drop across the Al_2O_3 film is lower than expectance and the influence of the electric field stress is not as severe as the un-NH_3 treatment Al_2O_3 samples. As the result, it will enhance the Q_{BD} for NH_3 treated Al_2O_3 samples.

It is important to study the conduction mechanisms of leakage current in Al_2O_3 film to improve its electrical and dielectric properties. Typically, two possible effects are in the metal-insulator interface, one is Schottky effect, the other is Frenkel-Poole effect. The Schottky-Richardson emission generated by the thermionic effect is caused by the electron transport across the potential energy barrier via field-assisted lowering at a metal-insulator interface. The leakage current equation is:

$$J = A^* T^2 \exp\left(\frac{\beta_s E^{1/2} - \phi_s}{k_B T}\right)$$

where $\beta_s = (e^3 / 4\pi\varepsilon_0\varepsilon)^{1/2}$, A^* effective Richardson constant,ϕ_s the contact potential barrier. We

can find the slope of the leakage current equation.

$$\ln J = \frac{\beta_s}{k_B T}\sqrt{E} + \left[\ln(A^* T^2) - \frac{\phi_s}{k_B T}\right]$$

$$slope = \frac{\beta_s}{k_B T}$$

The Frenkel- Poole (F-P) emission is due to field-enhanced thermal excitation of trapped electrons in the insulator into the conduction band. The leakage current equation is:

$$J = J_0 \exp\left(\frac{\beta_{FP} E^{1/2} - \phi_{PF}}{k_B T}\right)$$

where $J_0 = \sigma_0 E$ is the low-field current density, σ_0 the low-field conductivity, $\beta_{FP} = (e^3/\pi\varepsilon_0\varepsilon)^{1/2}$,e the electronic charge,ε_0 the permittivity of free space,ε the high frequency relative dielectric constant, T absolute temperature ,E the applied electric filed, K_B the Boltzmann constant,ϕ_{PF} the contact potential barrier. We can find the slope of the leakage current equation.

$$\ln J = \frac{\beta_{FP}}{k_B T}\sqrt{E} + \left[\ln(J_0) - \frac{\phi_{PF}}{k_B T}\right]$$

$$slope = \frac{\beta_{FP}}{k_B T}$$

From the equations as shown above, leakage current behaviors of insulate films can be investigated further on the leakage current density (J)-electric field (E) characteristics such as ln J vs. $E^{1/2}$ plots. The plot of the nature log of leakage current density versus the square root of the applied electric field was observed. It is found that the leakage current density is linearly related to square root of the applied electric field. The linear variations of the current correspond either to Schottky emission or to Frenkel-Poole conduction mechanism. For trap states with Coulomb potentials, the expression is virtually identical to that of the Schottky emission. The barrier height, however, is the depth of the trap potential well, and the quantity β_{FP} is larger than in the case of Schottky emission by a factor of 2. Distinction between the two processes can be done by comparing the theoretical value of β with the experimental one obtained by calculating the slope of the curve ln J-$E^{1/2}$. The dielectric constant of Al $_2O_3$ is 7.63 at PDA O_2 ambient and 8.29 at PDA N_2 ambient extracted by Fig. 20, the theory β values are 4.40×10^{-23} for Frenkel-Poole and 2.20×10^{-23} for Schottky after PDA in an O_2 ambient and the theory β values are 4.22×10^{-23} for Frenkel-Poole and 2.11×10^{-23} for Schottky after PDA in a N_2 ambient. Table 1 (a) and (b) shown the experimental β and Schottky barrier high of Al_2O_3 samples with NH_3 and without NH_3 treatment after PDA 900℃ in an O_2 ambient and after PDA 900℃ in a N_2 ambient, respectively. Fig. 18 (a) and (b) show the conduction mechanism fitting of Al_2O_3 samples with NH_3 and w/o NH_3 treatment after PDA 900℃ in an O_2 ambient and after PDA 900℃ in a N_2 ambient, respectively. We find the conduction mechanism in Al_2O_3 thin film is dominated by Schottky

conduction.

(C) Pre- and Post-corroded Fiber Structure in HF Vapor Environment

Figure 20 shows the fiber structure of PTFE-fiber and glass-fiber after the HF vapor corrosion. The pre- and post-corroded fiber structure of PTFE did not reveal any difference and this meant the PTFE-fiber was resistive for HF vapor. On the contrary, the fiber structure of glass-fiber shown in Fig. 20(b) displayed the serious degradation in HF vapor environment. The glass-fiber was inevitable to be corroded due to the strong reduction of HF to glass. It is worthy to notice that the corrosion of glass-fiber may release the boron and organic contaminants contained in glass-fiber ULPA filter, thus causing the degradation of device characteristics. Therefore, the PTFE ULPA filter is suitable to be used in acid vapor environment.

(D) Air Sampling Results in HF Vapor Environment

Figure 21 is the ICP-MS analysis results of metals and boron for different filter modules in HF vapor environment. The PTFE and the glass-fiber ULPA filter can effectively filter the metals including Na, K, Ca, Mg and Al. The CB with the PTFE and the GF ULPA filter, however, showed higher concentration of Fe ions than CR. It was suggested that the steel construction of clean bench corroded by HF vapor, releasing the Fe ions to air. Besides, the CB with GF filter showed large concentration of boron than the CB with PTFE filter. This may due to the corrosion of glass-fiber in HF vapor, releasing the boron atoms contained in glass-fiber as mentioned above. The detail analysis results of ICP-MS are listed in Table 4.

The organic compounds were considered to be another contamination the glass-fiber will release in HF vapor. Figure 22 shows the analysis results of GC/MS. It was found that all the organic contaminants were removed in the CB with PTFE filter. But for the CB with GF filter, high concentration of organic contaminants appeared. According to our study in Chapter 2, these organic contaminants may come from the binder in GF ULPA filter. In HF vapor environment, the degradation of glass-fiber will release more organic contaminants as show in Fig. 22. Table 5 shows the detail analysis results of GC/MS.

IV. Conclusion

In this thesis, characteristics and reliability of Al_2O_3 gate dielectrics with pre-deposition NH3 treatment and rapid thermal annealing in O_2 and N_2 ambient have been investigated. Several important phenomena were observed and summarized as follows. PDA can effectively reduce leakage current. For the samples with PDA at O_2 ambient, the interfacial layer increases with the higher PDA temperature. It is obviously that O_2 penetration will induce the increasing of the interfacial layer at Al_2O_3/Si-substrate and higher annealing temperature will speed up interface layer growth rate. For samples with PDA in a N_2 ambient, the void–defect of sputtered Al_2O_3 film will be eliminated. The as deposited Al_2O_3 film shows larger roughness, and after PDA it will become smoother. However, with higher PDA temperature, surface rough will slightly increase.

The surface NH_3 treatment can lower the CET value and reduce the leakage current. In addition, the dielectric reliability was enhanced with NH_3 treatment. The low Weibull slope of Al_2O_3 film may result from sputter-induced defects causing weak spots. Significant process improvements are necessary to enhance dielectric quality, such as MOCVD, ALCVD. The conduction mechanism in Al_2O_3 film was investigated by the various temperature measurement

and fitting. The conduction mechanism in Al_2O_3 thin film is dominated by Schottky conduction which occurred for insulators with fewer defects and a more perfect metal-insulator interface. Samples after NH_3 treatment will have higher barrier high to reduce the leakage current.

The qualitative and quantitative analyses of AMC in the CB with different filter module in HF vapor environment were investigated. The experimental results showed that the GF ULPA filter will release boron and organic contaminants in HF vapor environment, while the PTFE ULPA filter still maintained low concentration of contaminants. The effects of the materials from which air filters are made on device characteristics were also investigated. The glass-fiber ULPA filter released AMC when exposed in an HF vapor environment. These contaminants included organic compounds and boron trace dopants and degraded the device characteristics. In contrast, the HF vapor did not affect the PTFE ULPA filter. These results suggested that the PTFE fiber can be a good ULPA filter material for providing a very clean environment.

計畫成果自評

本計畫為三年期計畫，依原訂計畫第二年目標，本計畫完成了奈米級閘極介電層關鍵製程技術之研發以及奈米級微污染分析防治，相關論文仍在投稿當中。在奈米級閘極介電層關鍵製程技術之研發方面，開發出未來奈米元件用之高介電常數 Al_2O_3 閘極介電層，並研究其特性及最佳化條件，此高介電氧化鋁薄膜經過 NH_3 的前處理及 N_2 RTA 製程退火處理，可獲得最佳電性，適用於未來的奈米元件製程；最後在奈米級微污染分析防治方面，我們以氫氟酸加速實驗檢驗了目前無塵室空氣濾網的適用性，並採用新開發之 PTFE 濾網來控制無塵室中之硼微污染跟有機污染。本計畫未來一年將以前兩年為基礎，繼續進行氧化鋁和臭氧水製程之奈米閘極絕緣層跟無塵室微污染對於奈米元件之影響等相關研究。

Si-Substrate

1. RCA clean and LOCOS

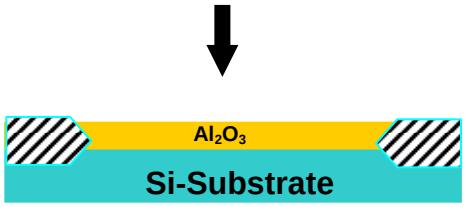

2. Al_2O_3 deposition (60Å)

by Reactive Sputter

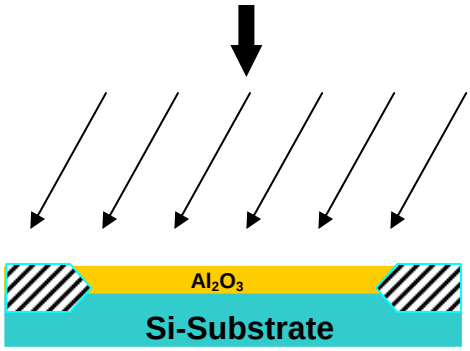

3. RTA treatment N_2/ 5 slm/30 sec or

O_2/ 5 slm/30 sec 750℃ , 850℃ ,950℃

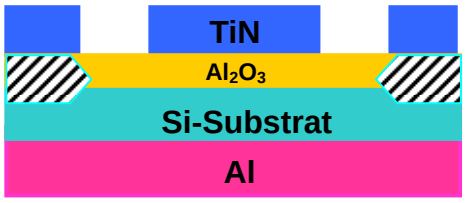

4. Top electrode formation TiN-2000 Å &

Backside contact formation Al -5000Å

Fig.1 Process flows of experimental samples

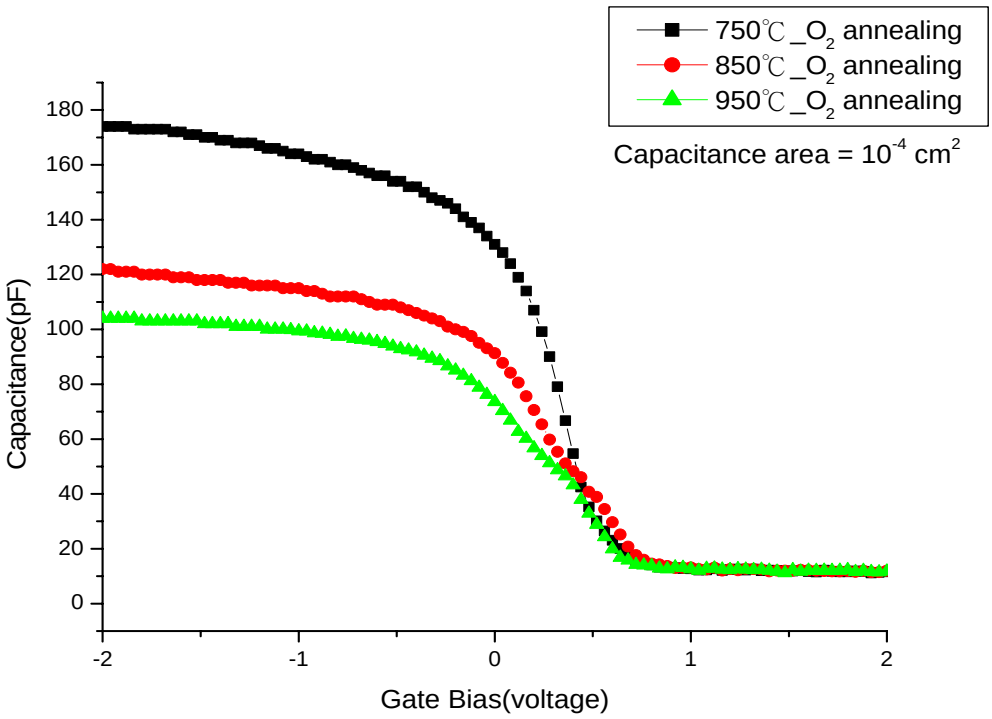

Fig.2 The C-V curves of Al_2O_3 samples annealing in an O_2 ambient

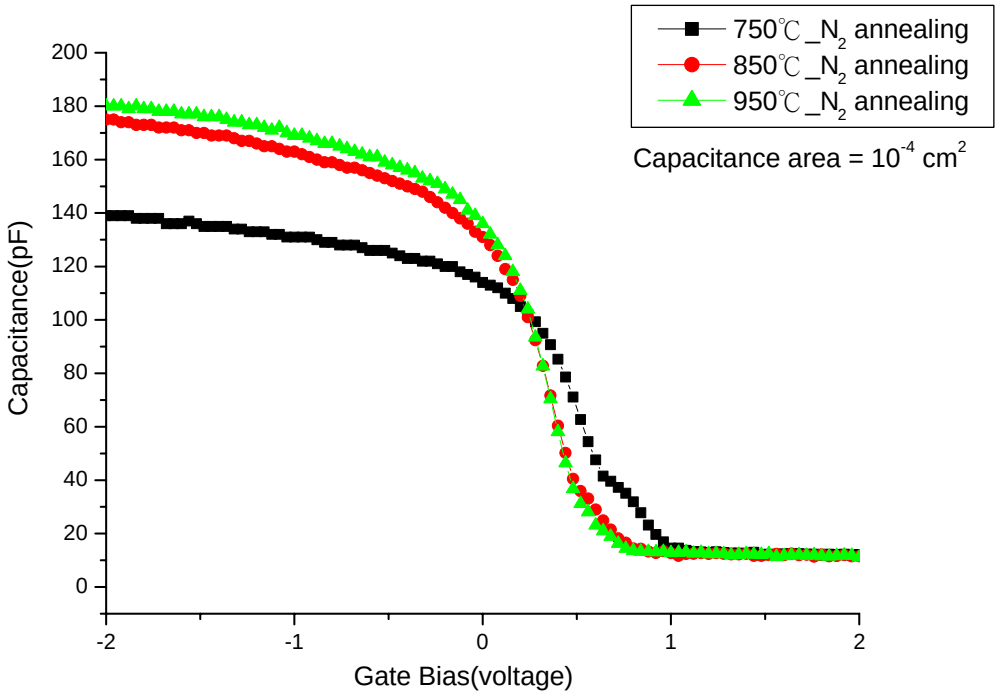

Fig. 3 The C-V curves of Al_2O_3 samples annealing in a N_2 ambient

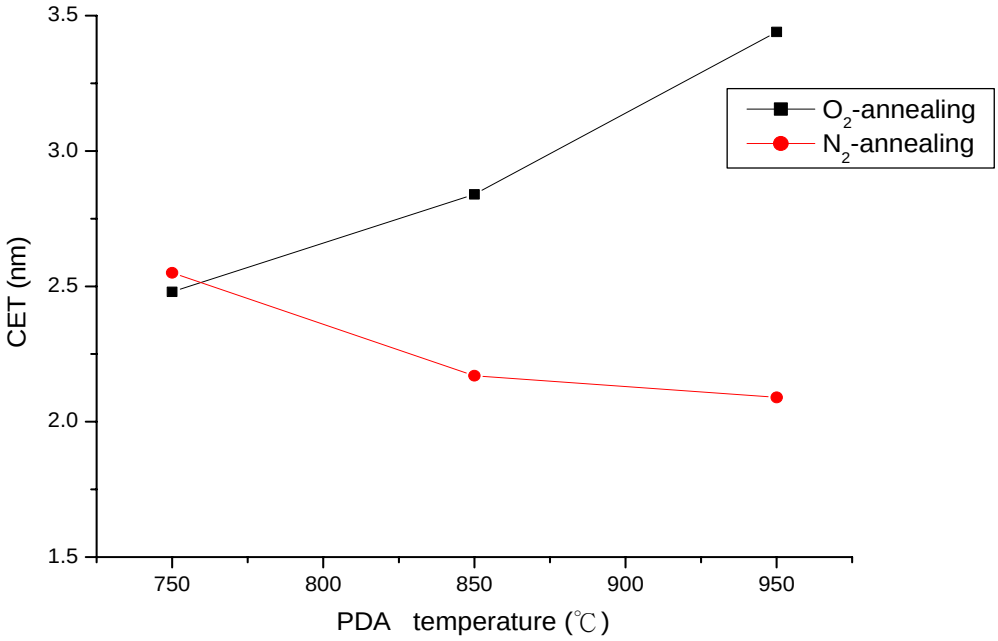

Fig. 4 The CET of Al_2O_3 samples after various post annealing temperature 750℃, 850℃, 950℃

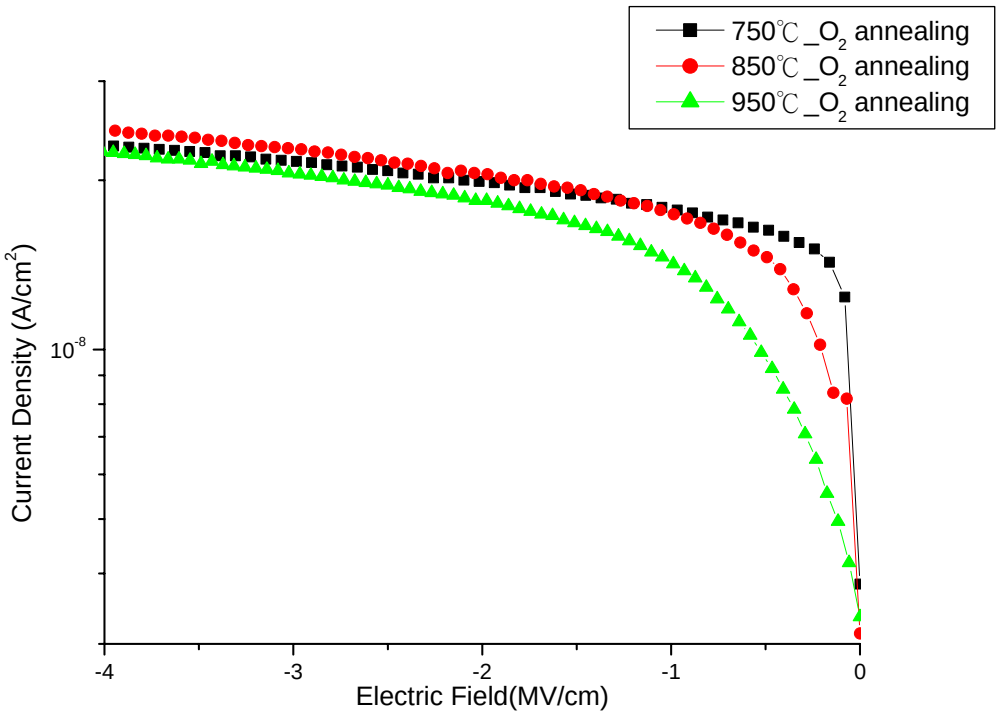

Fig. 5 The J-E curves of Al_2O_3 samples with various PDA temperature in an O_2 ambient.

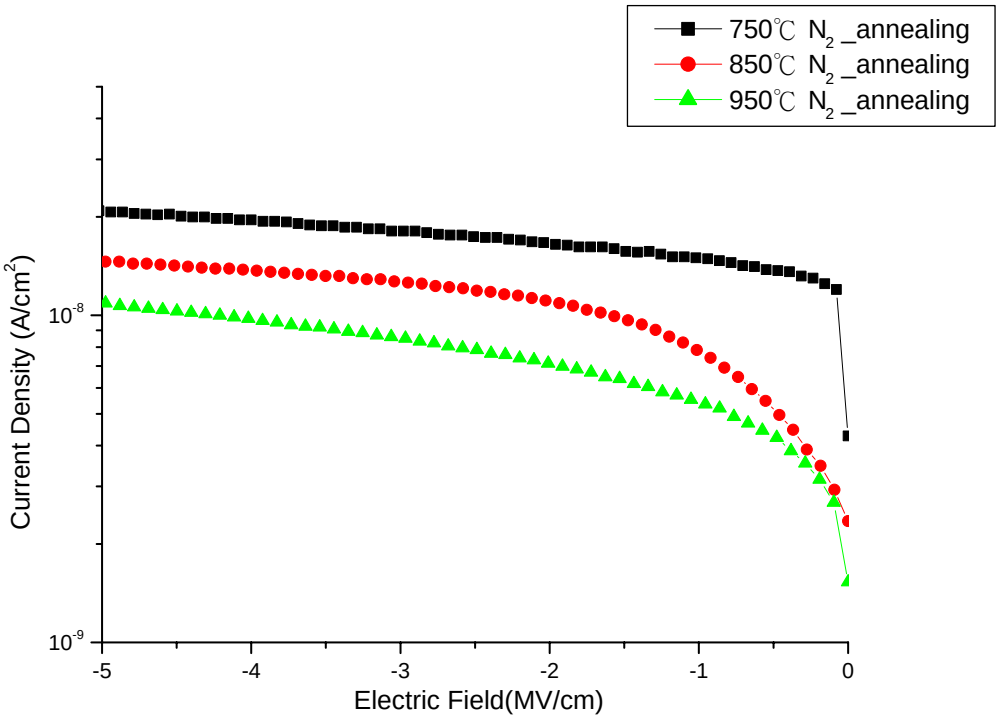

Fig. 6 The J-E curves of Al_2O_3 samples with various PDA temperature in a N_2 ambient.

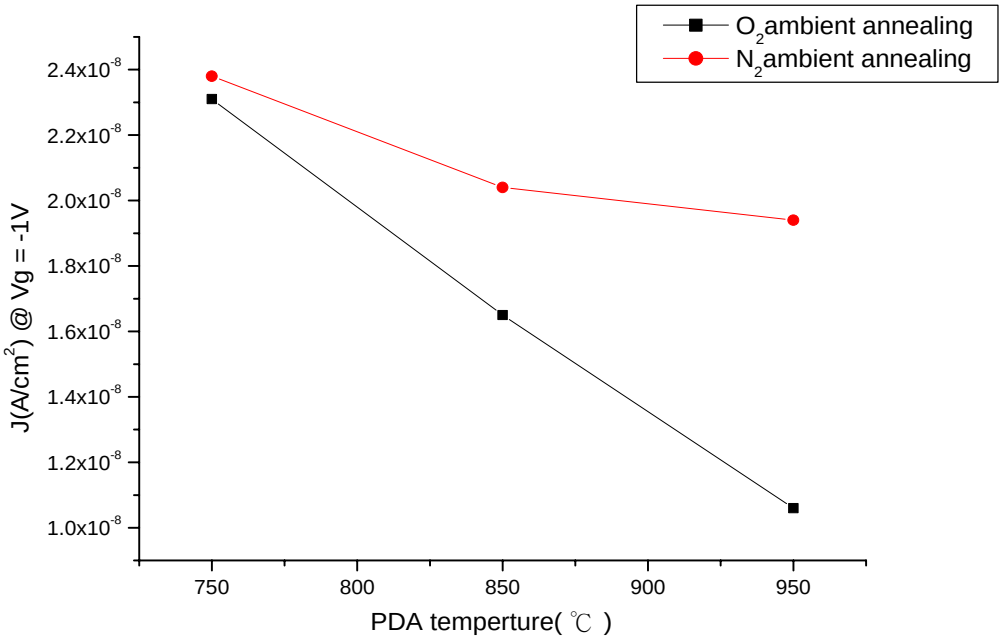

Fig. 7 The J at Vg= -1 V of Al_2O_3 samples with various PDA temperature

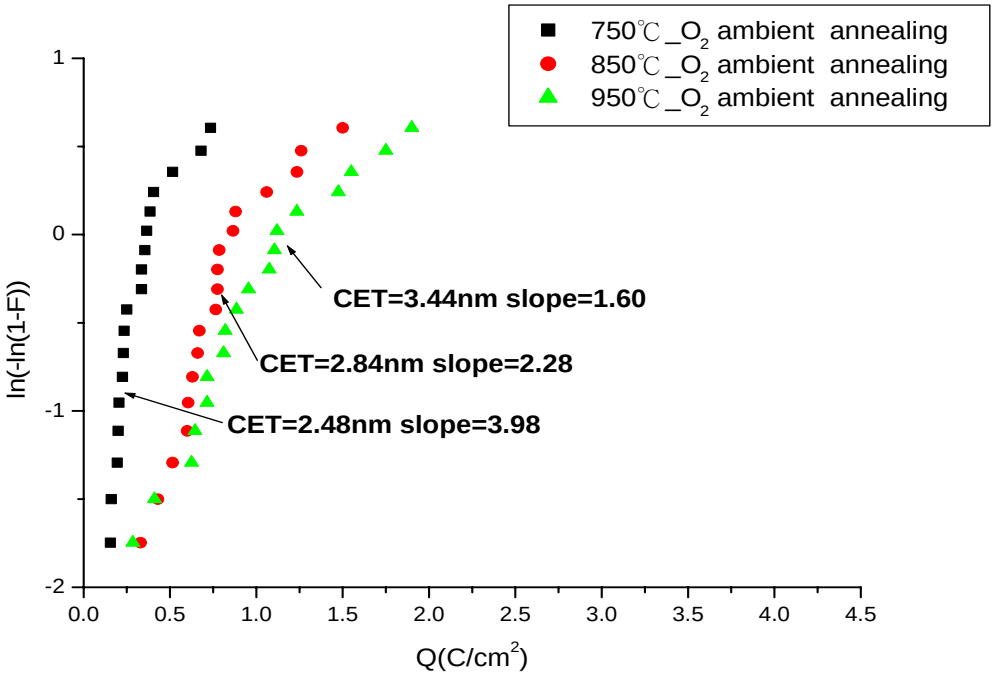

Fig. 8 The Weibull plot versus the charge to breakdown Q (C/cm^2) of Al_2O_3 samples with various PDA temperature in an O_2 ambient.

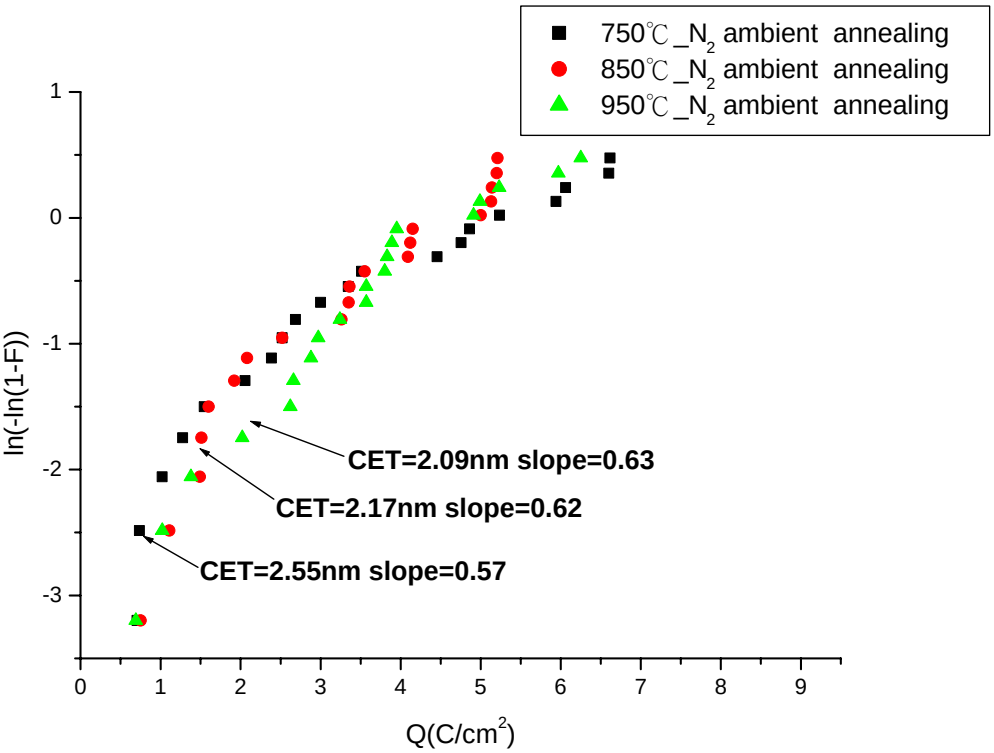

Fig. 9 The Weibull plot shows the charge to breakdown Q (C/cm^2) of Al_2O_3 samples with various PDA temperature in a N_2 ambient.

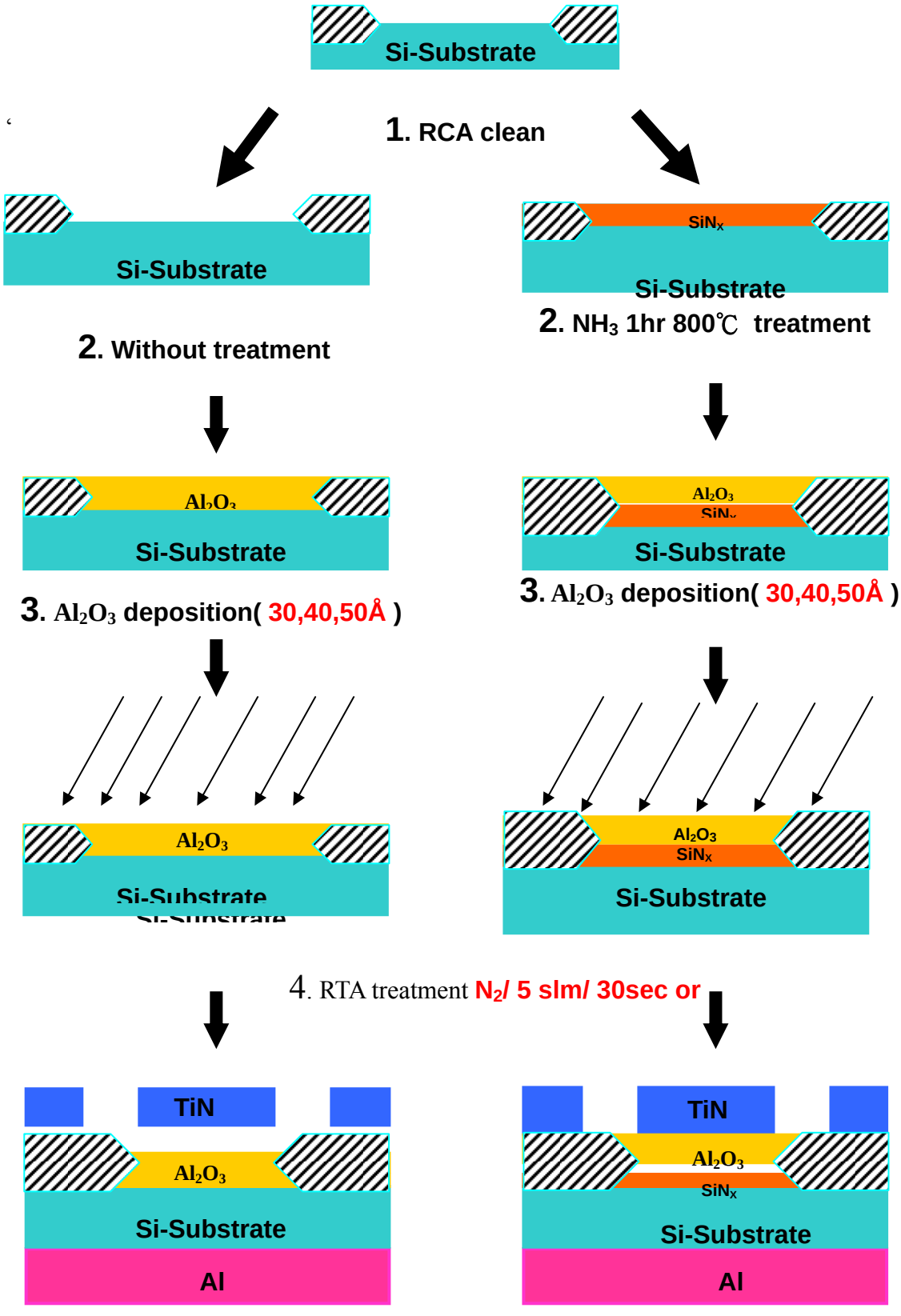

5. Top electrode formation TiN -2000 Å pattern contact

Fig.10 Process flows of experimental samples

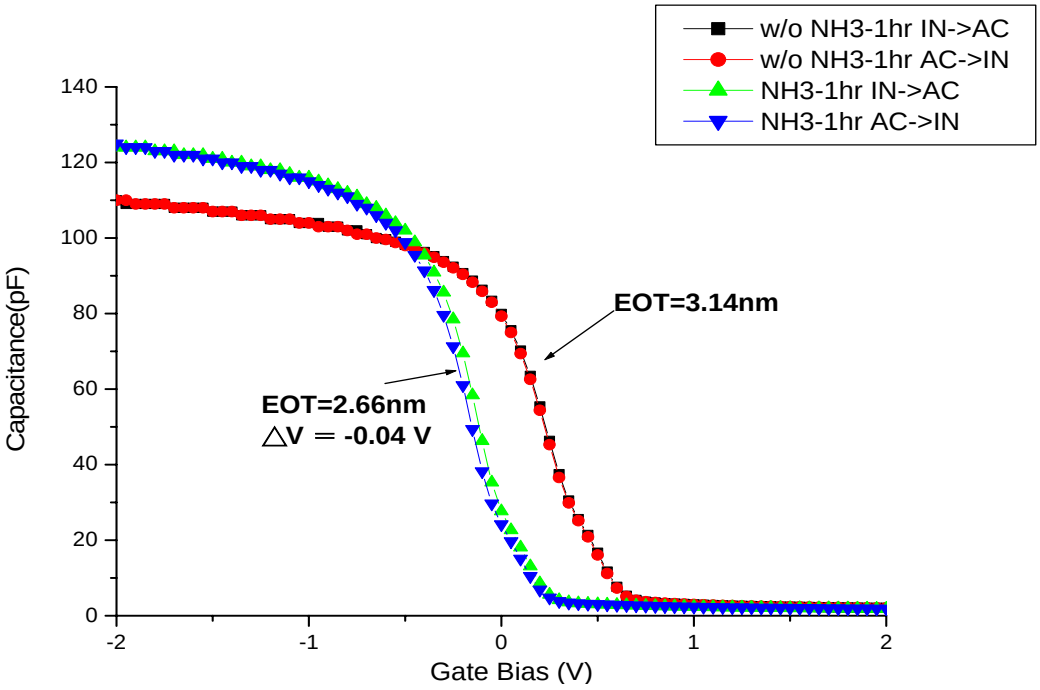

Fig. 11: C-V curve of Al_2O_3 sample with surface treatment compare to Al_2O_3 sample without surface treatment after PDA 900℃ in an O_2 ambient

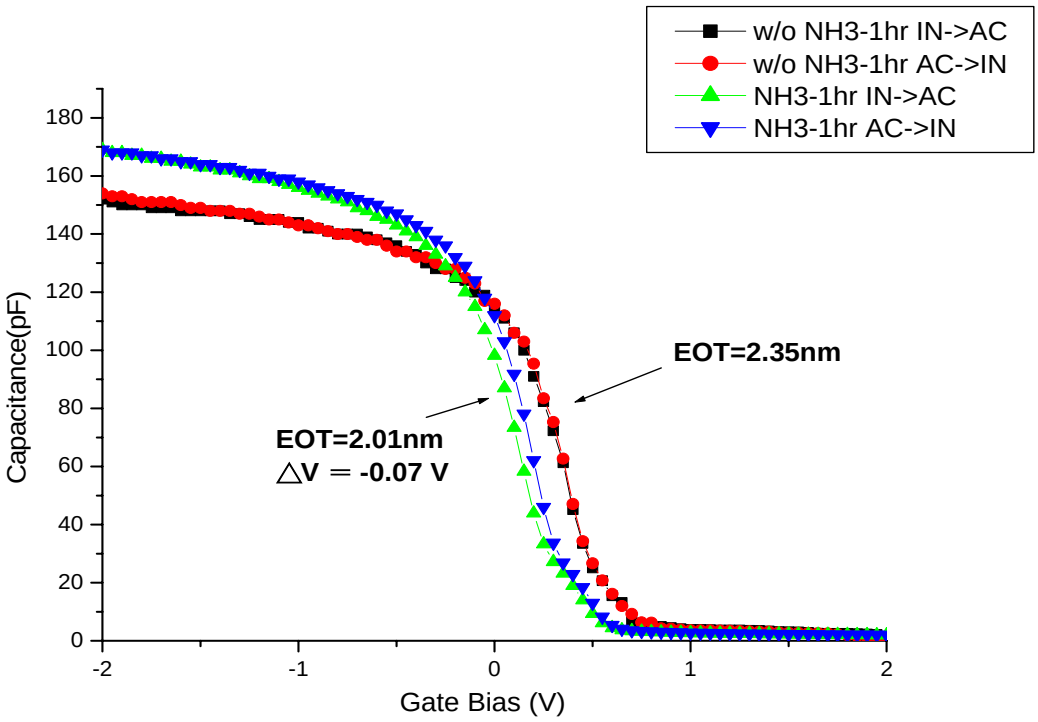

Fig. 12: C-V curve of Al_2O_3 sample with surface treatment compare to Al_2O_3 sample without surface treatment after PDA 900℃ in a N_2 ambient

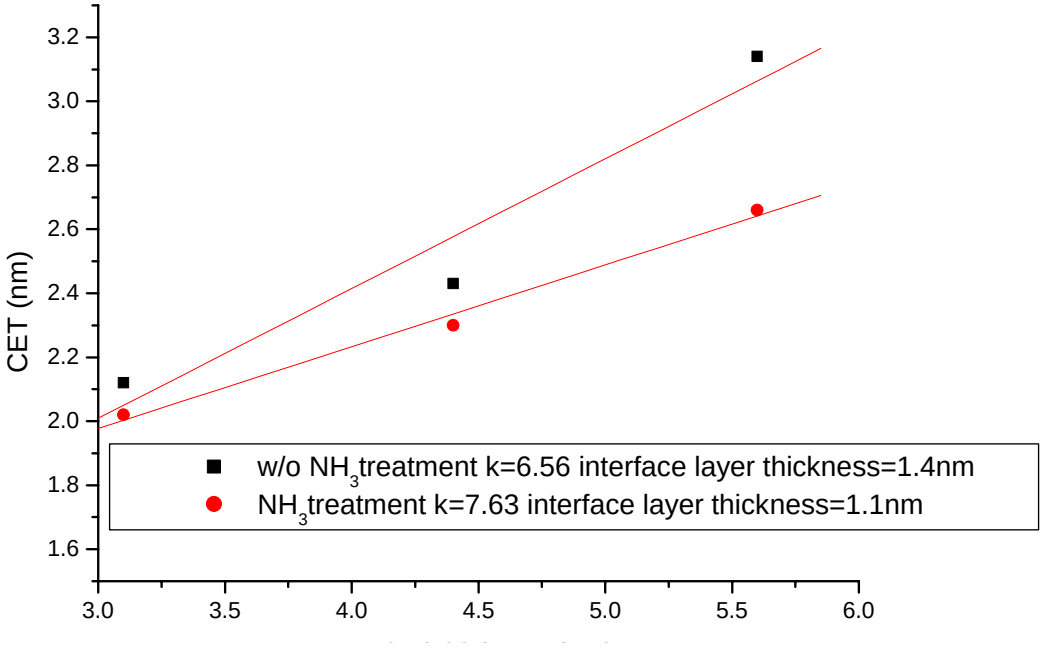

Fig. 13: CET versus Optical thickness of Al_2O_3 sample with surface treatment compare to Al_2O_3 sample without surface treatment after PDA 900℃ in an O_2 ambient

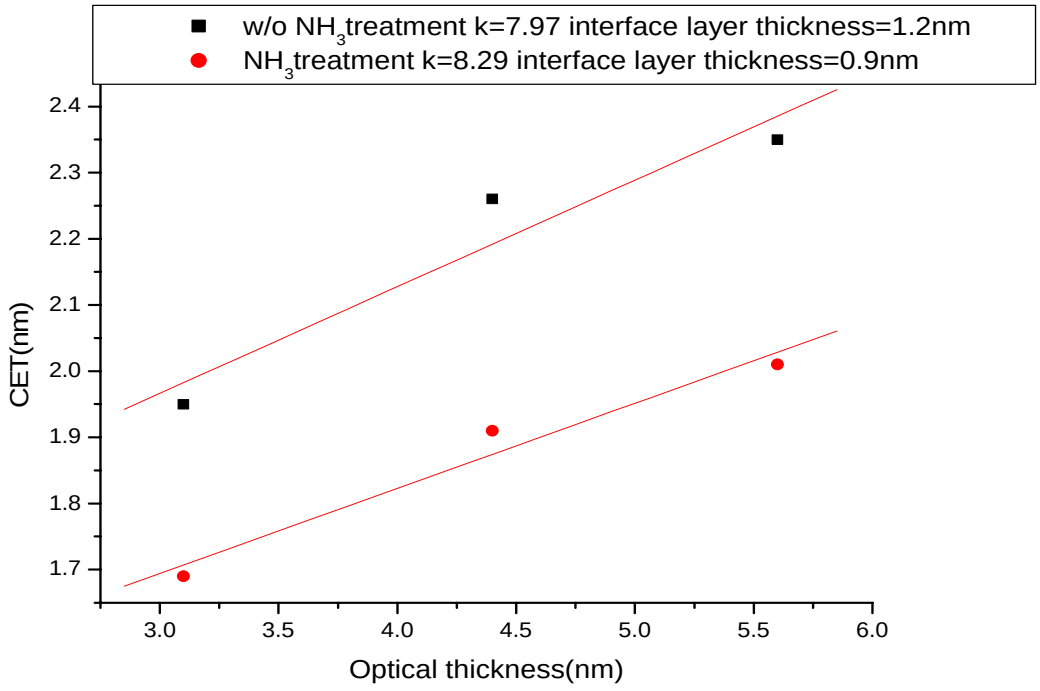

Fig. 14: CET versus Optical thickness of Al_2O_3 sample with surface treatment compare to Al_2O_3 sample without surface treatment after PDA 900℃ in a N_2 ambient

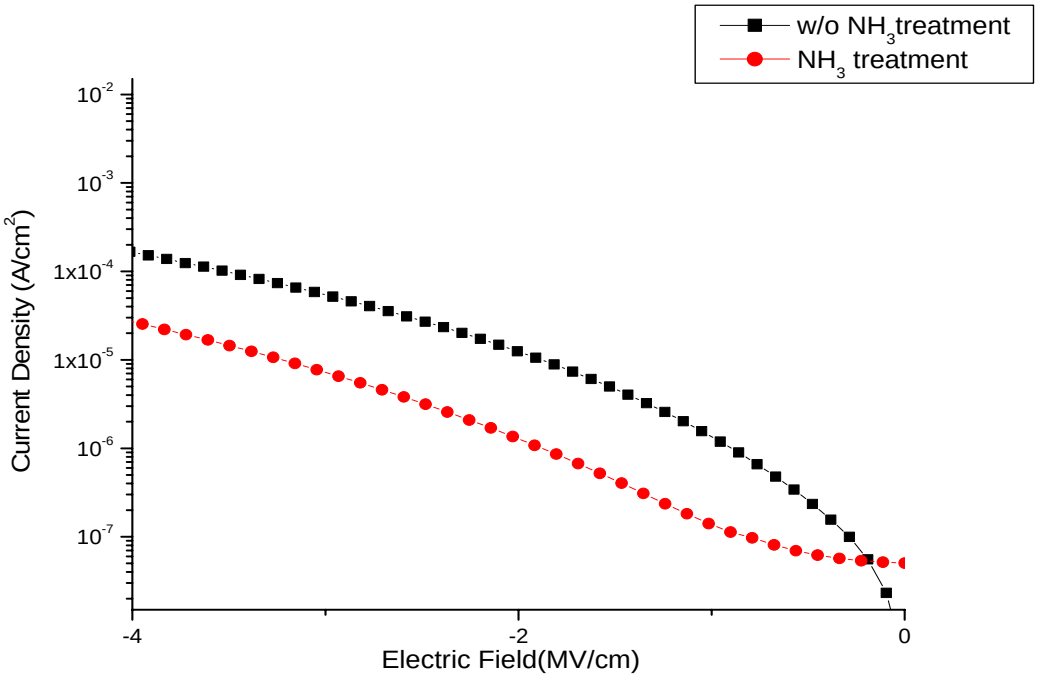

Fig. 15(a): The gate leakage current density (J) versus electric field (E) curves for NH_3 nitrided and w/o NH_3 nitrided after PDA 900℃ in an O_2 ambient

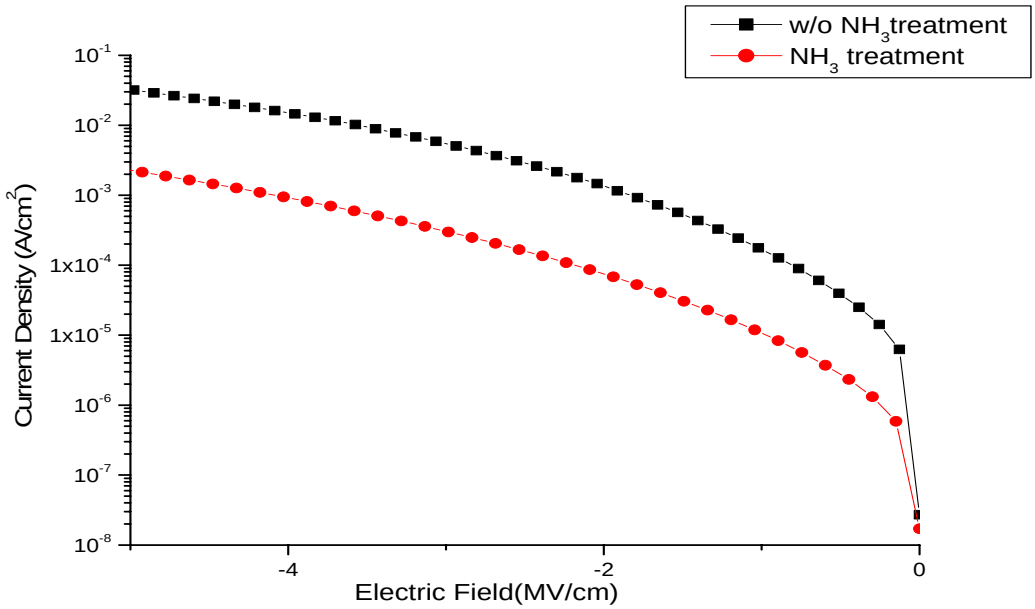

Fig. 15(b): The gate leakage current density (J) versus electric field (E) curves for NH_3 nitrided and w/o NH_3 nitrided after PDA 900℃ in a N_2 ambient

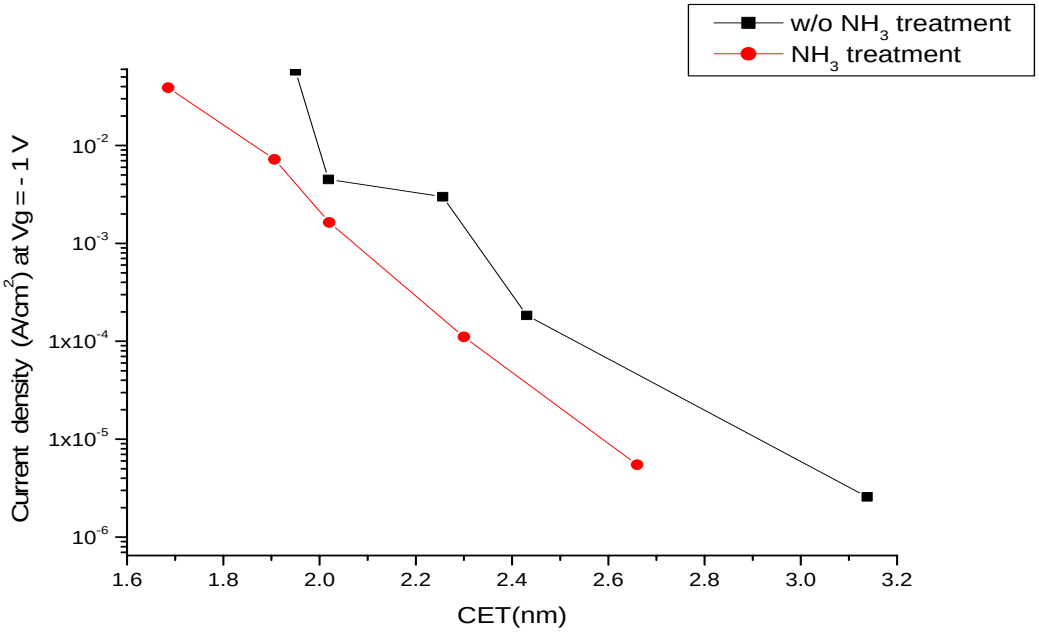

Fig. 16 Current density at Vg = -1Vversus CET curves for NH3 treatment and without NH3 treatment.

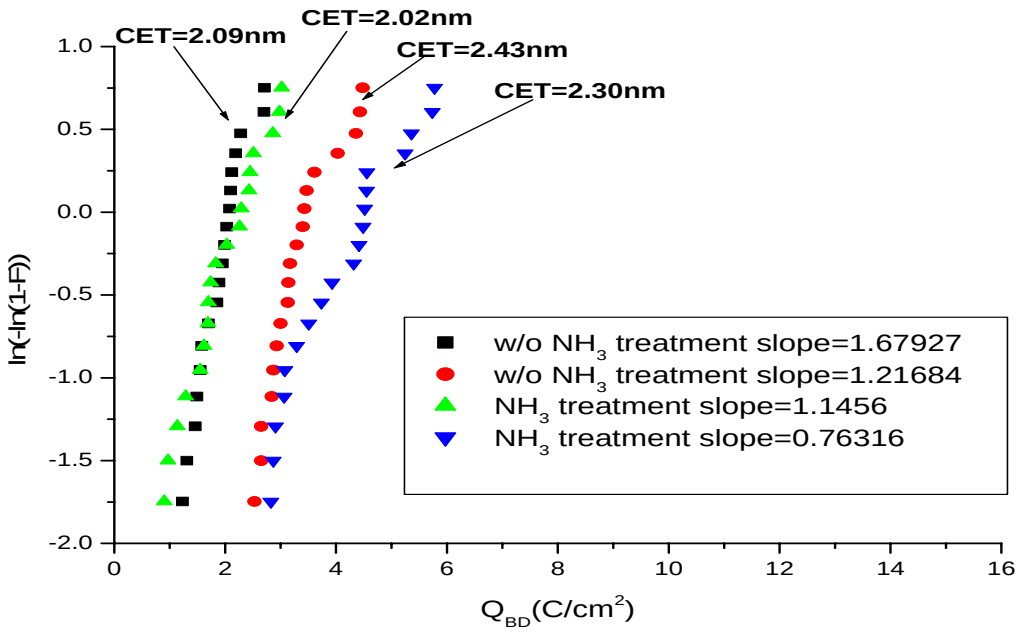

Fig. 17 (a)The weibull plot shows charge to breakdown for Al_2O_3 samples with NH_3 and w/o NH_3 treatment at PDA after PDA 900℃ in an O_2 ambient

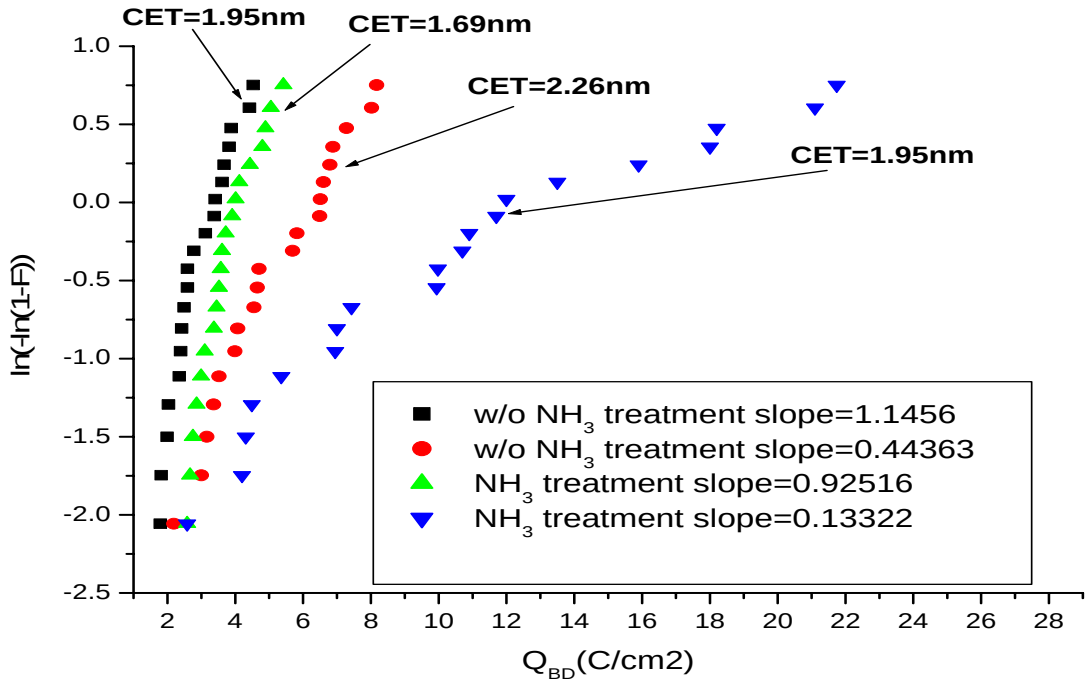

Fig. 17 (b)The weibull plot shows charge to breakdown for Al_2O_3 samples with NH_3 and w/o NH_3 treatment at PDA after PDA 900℃ in a N_2 ambient

	w/o NH_3 treatment		With NH_3 treatment	
	βexp	Schottky barrier high	βexp	Schottky barrier high
25℃	$1.88*10^{-23}$	0.71ev	$2.37*10^{-23}$	0.97ev
50℃	$2.18*10^{-23}$	0.72 ev	$2.37*10^{-23}$	1.06ev
75℃	$2.48*10^{-23}$	0.70 ev	$2.49*10^{-23}$	1.13ev
100℃	$2.59*10^{-23}$	0.74 ev	$2.59*10^{-23}$	1.20ev
125℃	$2.71*10^{-23}$	0.70 ev	$2.71*10^{-23}$	1.28ev

Table. 1(a) The experimental β and Schottky barrier high of Al_2O_3 samples with NH_3 and w/o NH_3 treatment after PDA 900℃ in a O_2 ambient

	w/o NH_3 treatment		With NH_3 treatment	
	βexp	Schottky barrier high	βexp	Schottky barrier high
25℃	$1.93*10^{-23}$	0.73 ev	$1.98*10^{-23}$	0.83ev
50℃	$1.83*10^{-23}$	0.65 ev	$2.15*10^{-23}$	0.89ev
75℃	$2.04*10^{-23}$	0.69 ev	$2.32*10^{-23}$	0.96ev
100℃	$2.13*10^{-23}$	0.72 ev	$2.45*10^{-23}$	1.03ev
125℃	$2.01*10^{-23}$	0.77 ev	$2.61*10^{-23}$	1.10ev

Table.1(b) The experimental β and Schottky barrier high of Al_2O_3 samples with NH_3 and w/o NH_3 treatment after PDA 900℃ in a N_2 ambient

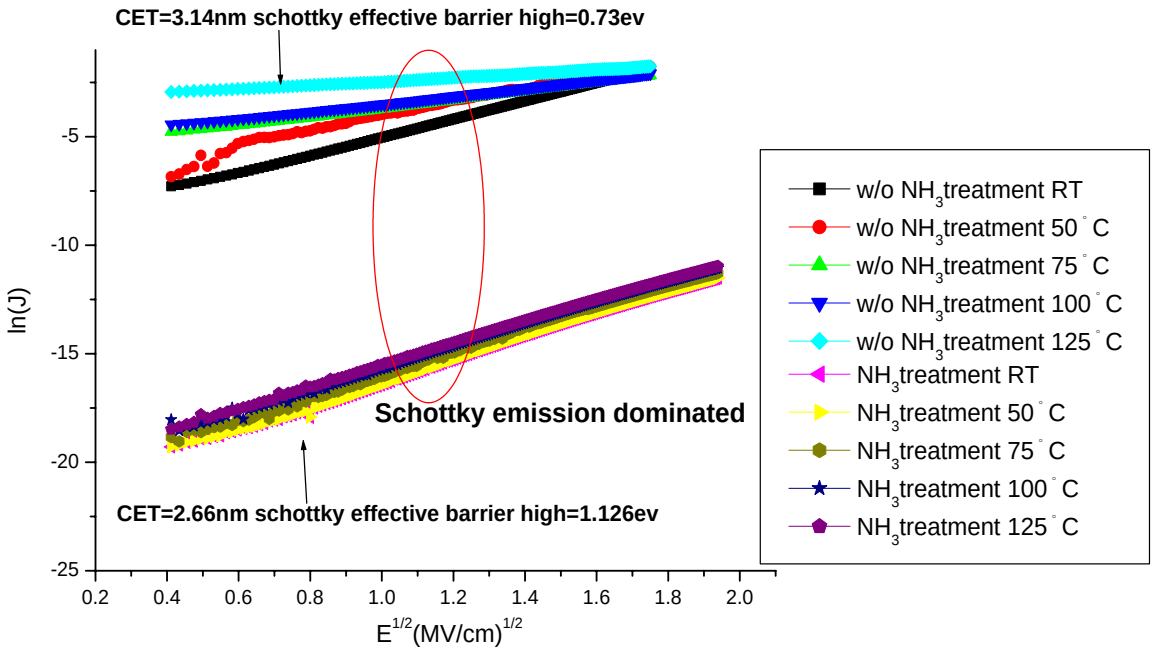

Fig.18(a) The conduction mechanism fitting of Al_2O_3 samples with NH_3 and w/o NH_3 treatment after PDA 900℃ in an O_2 ambient

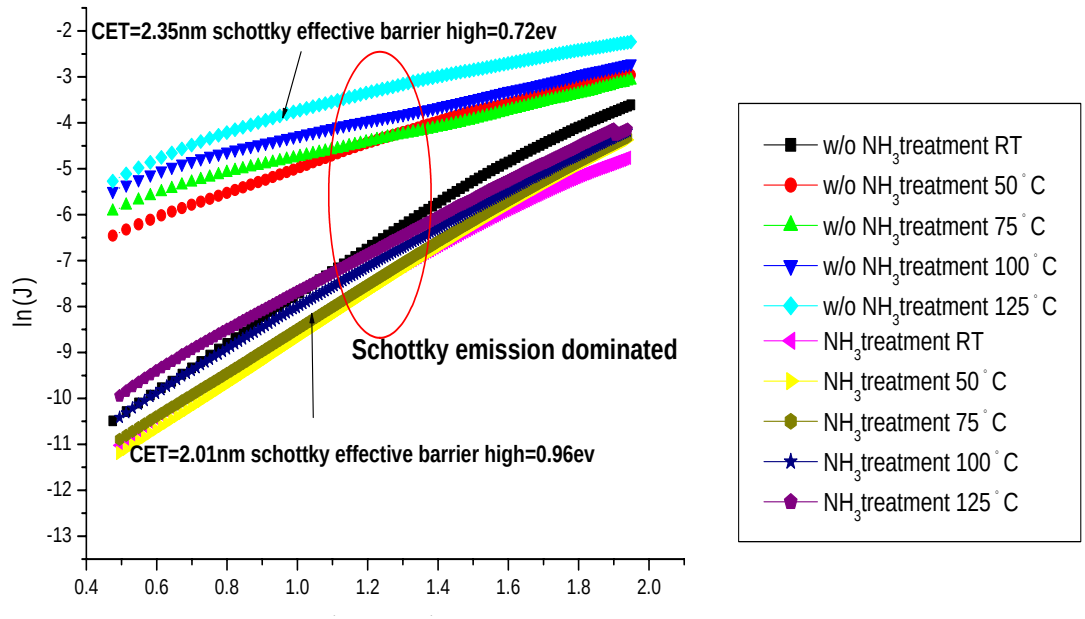

Fig.18(b) The conduction mechanism fitting of Al_2O_3 samples with NH_3 and w/o NH_3 treatment after PDA 900℃ in a N_2 ambient

TABLE 2

Summary of Air Sampling Experimental Conditions

Contamination Type	Sampling Equipments	Flow Rate	Sampling Time	Analysis Method
Organic Compounds	TENAX Tube	100 mL/min.	5 hrs	GC/MS (Gas Chromatograph Mass Spectrometer)
Metals & Boron	Impinger	2 L/min.	72 hrs	ICP-MS (Inductively Coupled Plasma Mass Spectrometer)

Bench Condition
Filter module: 1. PTFE ULPA filter + Chemical filter
2. Glass-Fiber ULPA filter + Chemical filter
Air flow rate: 0.4 m/s
Turnover rate: 5%
Temperature: 23 ℃
1ppm HF Vapor

TABLE 3

Summary of Wafer Sampling Experimental Conditions

Contamination Type	Exposing Location	Exposing Time	Analysis Method	Elements
Organic Compounds	CR and CB	24 hrs	TDS-APIMS (Thermal Desorption System – Atmospheric Pressure Ionized Mass Spectrum)	D3, D4, D5, D6, DEP, DBP, TEP, TBP, BHT
Metals	CR and CB	72 hrs	TRXRF (Total Reflection X-Ray Fluorescence)	Na, K, Ca, Mg, Fe, Ti, V, Cr, Mn, Co, Ni, Cu, Zn

Filter module: 1. PTFE ULPA filter + Chemical filter
2. Glass-Fiber ULPA filter + Chemical filter
Air flow rate: 0.4 m/s
Turnover rate: 5%
Temperature: 23 ℃
1ppm HF Vapor

TABLE 4
Air Sampling Results of Metals and Boron in HF Vapor Environment

Metals & Boron ($\mu g/m^3$)	CR	Detection Limit	CB_PTFE	Detection Limit	CB_GF	Detection Limit
Inlet Filter	-		Chemical Filter		Chemical Filter	
Main Filter	-		PTFE Filter		Glass-Fiber Filter	
Na	0.25	0.002	<0.004	0.004	<0.002	0.002
K	0.006	0.004	<0.004	0.004	<0.004	0.004
Ca	0.004	0.004	<0.004	0.004	<0.004	0.004
Mg	<0.004	0.004	<0.004	0.004	<0.004	0.004
Al	<0.004	0.004	<0.004	0.004	<0.004	0.004
Fe	<0.004	0.004	0.008	0.004	0.05	0.004
B	0.024	0.0008	0.0036	0.0008	0.062	0.0009

TABLE 5
Air Sampling Results of Organic Compounds in HF Vapor Environment

Organic Compounds ($\mu g/m^3$)	CR	Detection Limit	CB_PTFE	Detection Limit	CB_GF	Detection Limit
Inlet Filter	-		Chemical Filter		Chemical Filter	
Main Filter	-		PTFE Filter		Glass-Fiber Filter	
D3:$C_6H_{18}O_3Si_3$	2.1	0.03	<0.03	0.03	*1	0.03
D4:$C_8H_{24}O_4Si_4$	<0.07	0.07	<0.07	0.07	0.11	0.07
D5:$C_{10}H_{30}O_5Si_5$	0.34	0.03	<0.03	0.03	0.14	0.03
D6:$C_{12}H_{36}O_6Si_6$	0.04	0.03	<0.03	0.03	0.14	0.03
DEP:$C_{12}H_{14}O_4$	<0.03	0.03	<0.03	0.03	0.27	0.03
DBP:$C_{16}H_{22}O_4$	0.27	0.22	<0.22	0.22	1.4	0.22
TEP:$C_6H_{15}O_4P$	<0.03	0.03	<0.03	0.03	<0.03	0.03
TBP:$C_{12}H_{27}O_4P$	<0.03	0.03	<0.03	0.03	<0.03	0.03
BHT:$C_{15}H_{24}O$	<0.03	0.03	<0.03	0.03	0.04	0.03

*1: Can not separate organic compounds peaks

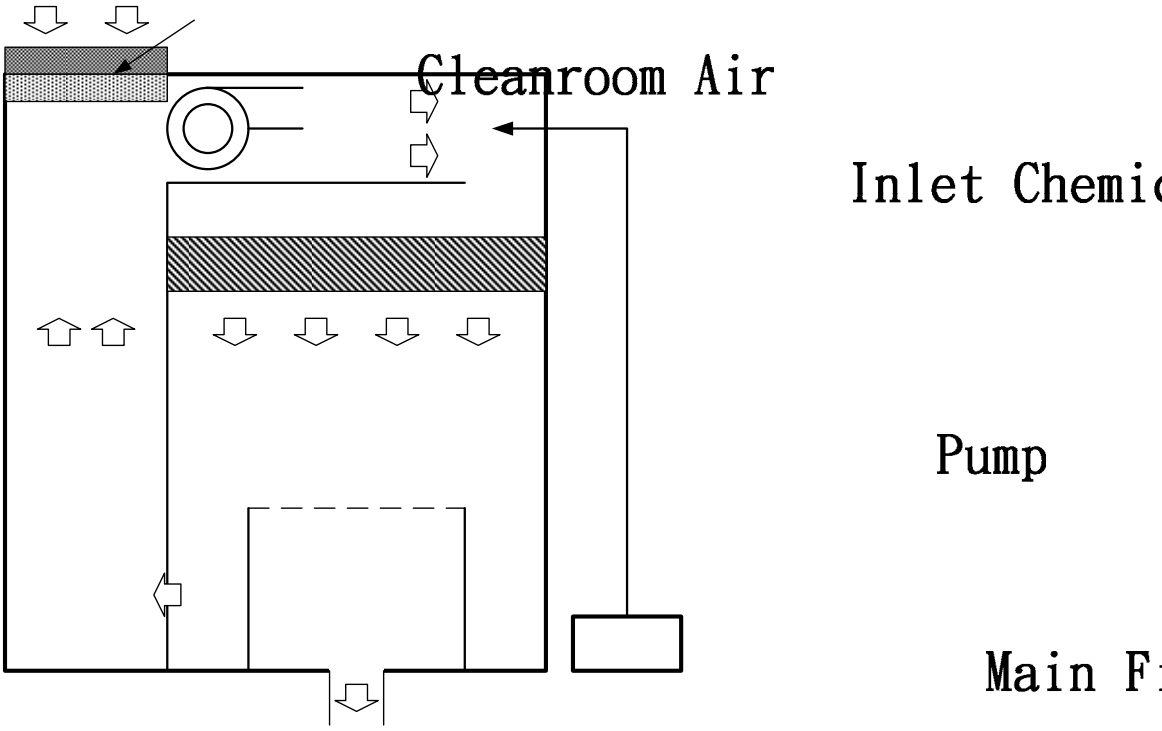

Fig. 19(a) Schematic diagram of specially designed clean bench with the HF vapor.

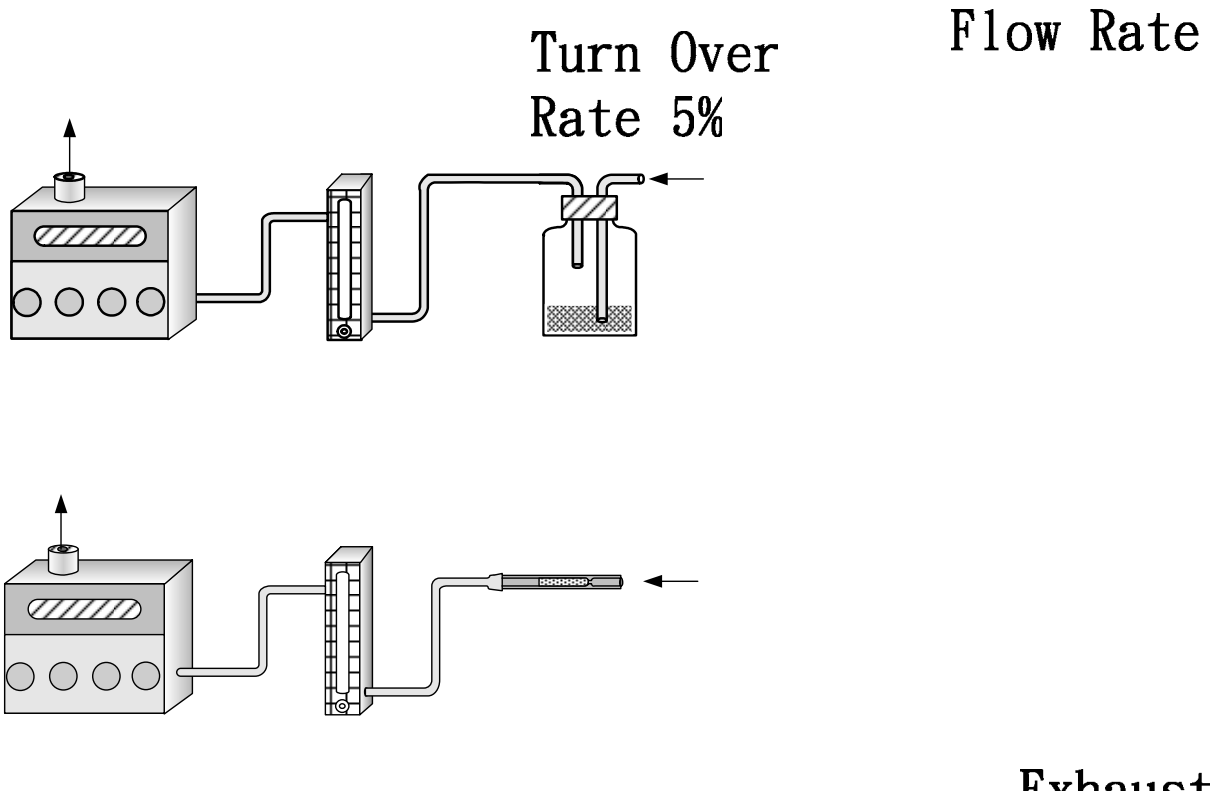

Fig. 19(b) Air sampling equipments used for the evaluation of metals and organic contaminations.

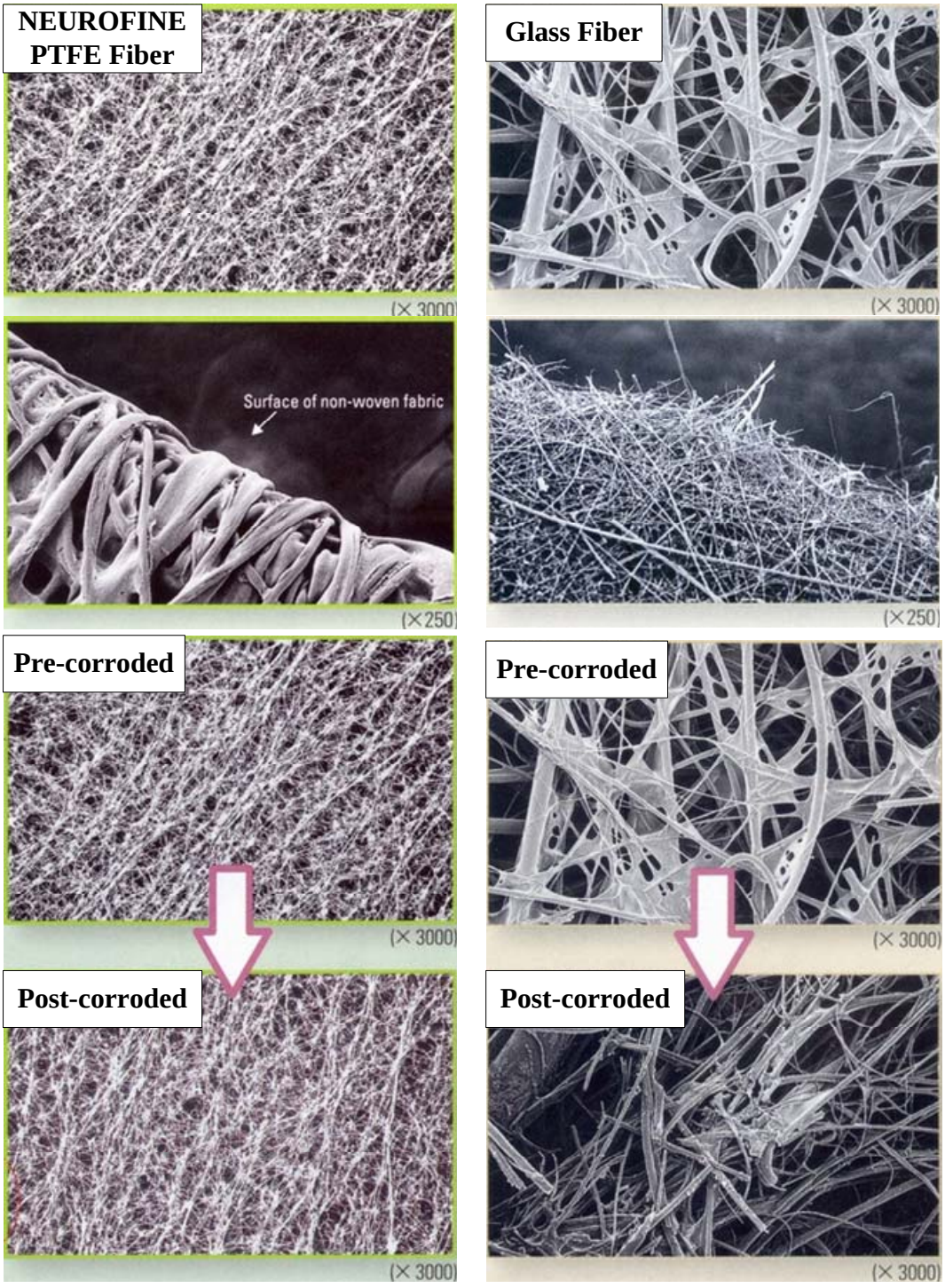

(a) (b)

Fig. 20 The SEM photographs of (a) PTFE-fiber and (b) Glass-fiber structures.

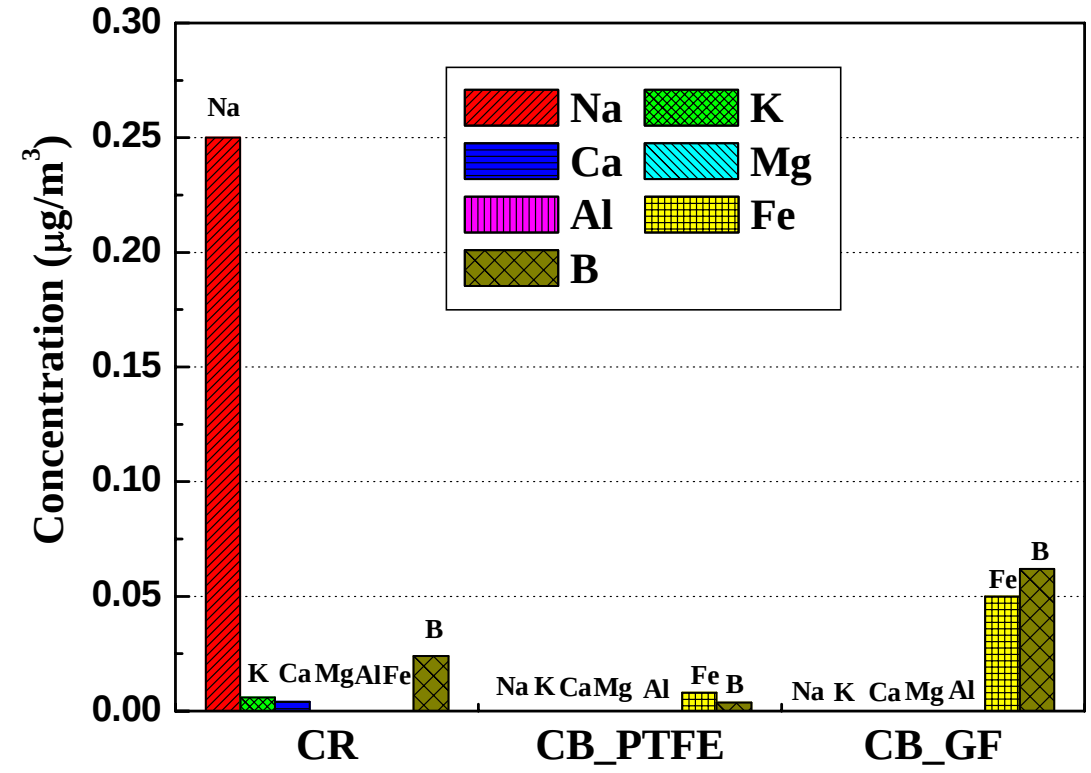

Fig. 21 Air sampling results of metals and boron in HF vapor environment.

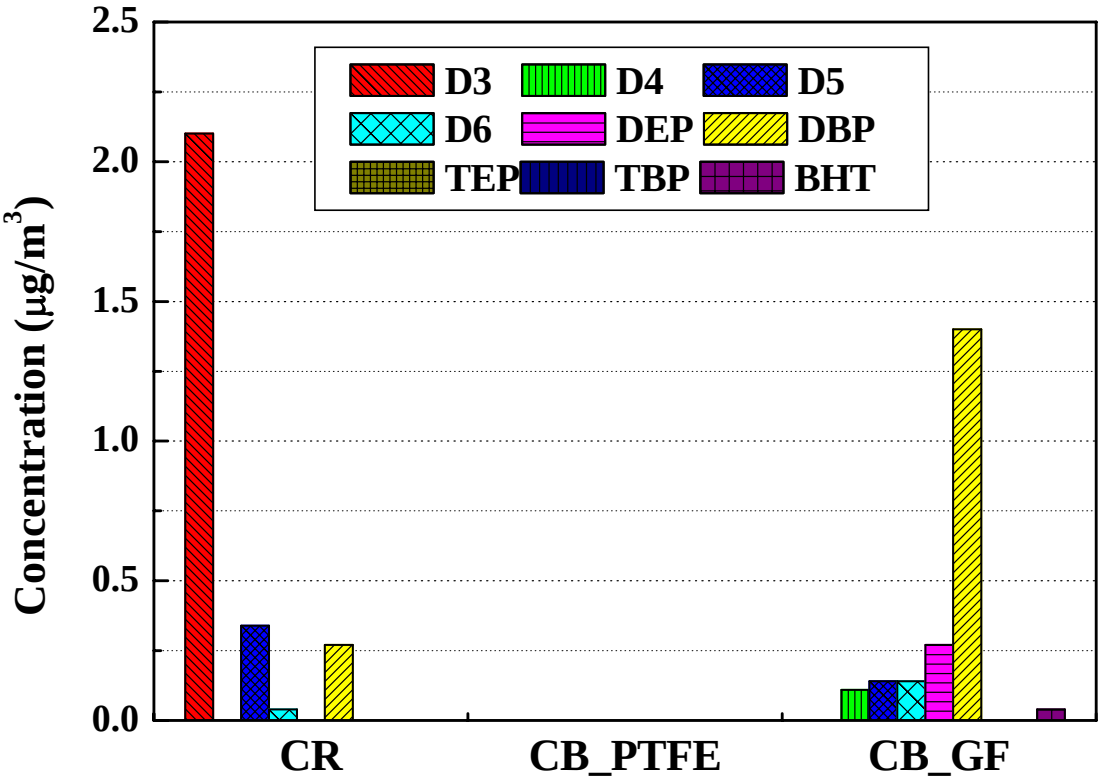

Fig. 22 Air sampling results of organic compounds in HF vapor environment.